

Marlim R3D: A realistic model for controlled-source electromagnetic simulations — Phase 2: The controlled-source electromagnetic data set

Jorlivan L. Correa¹ and Paulo T. L. Menezes²

ABSTRACT

Synthetic data provided by geoelectric earth models are a powerful tool to evaluate a priori a controlled-source electromagnetic (CSEM) workflow effectiveness. Marlim R3D (MR3D) is an open-source complex and realistic geoelectric model for CSEM simulations of the postsalt turbiditic reservoirs at the Brazilian offshore margin. We have developed a 3D CSEM finite-difference time-domain forward study to generate the full-azimuth CSEM data set for the MR3D earth model. To that end, we fabricated a full-azimuth survey with 45 towlines striking the north-south and east-west directions over a total of 500 receivers evenly spaced at 1 km intervals along the rugged seafloor of the MR3D model. To correctly represent the thin, disconnected, and complex geometries of the studied reservoirs, we have built a finely discretized mesh of $100 \times 100 \times 20$ m cells leading to a large mesh with a total of approximately 90 million cells. We computed the six electromagnetic field components (E_x , E_y , E_z , H_x , H_y , and H_z) at six frequencies in the range of 0.125–1.25 Hz. In our efforts to mimic noise in real CSEM data, we summed to the data a multiplicative noise with a 1% standard deviation. Both CSEM data sets (noise free and noise added), with inline and broadside geometries, are distributed for research or commercial use, under the Creative Common License, at the Zenodo platform.

INTRODUCTION

The marine controlled-source electromagnetic (CSEM) method is a risk-reduction tool that provides complementary information to seismic in the exploration of sedimentary basins (Constable and

Srnka, 2007). The CSEM method is routinely used for reservoir scanning and appraisal (e.g., Fanavoll et al., 2014; Løseth et al., 2014; Miotti et al., 2018). The CSEM interpretation workflow is heavily based on inversion and forward modeling for hypothesis testing. Until the recent past, the effectiveness of a given workflow was accomplished after the drilling results because there were not any geologic complex models available to serve as a benchmark.

Synthetic data produced by geoelectric earth models can be used as a priori to assess a CSEM workflow's effectiveness. Most of the available models are simplistic physical models with a known mathematical formulation (e.g., Orange et al., 2009; Ray et al., 2013; Yoon et al., 2016). These models are proper for software development, but they are usually inappropriate for describing the geologic complexity of the marine substrate adequately; consequently, they tend to impact the workflow of actual data interpretation negatively (Tseng et al., 2015). Recently, several authors have presented complex models (Bhuyian et al., 2010; Puzyrev et al., 2013; Colombo et al., 2018; Dunham et al., 2018), but they are, to our knowledge, proprietary models and thus may be of restricted use.

SEG recognized this issue and developed a particular project, the SEG Advanced Modeling (SEAM) Project, aimed at constructing realistic synthetic earth models. According to Fehler (2009), the SEAM Project's goal is to develop the science and technology of applied geophysics through a cooperative industry enterprise concentrated on subsurface model building and production of synthetic data sets for geophysical problems of importance to the hydrocarbon industry. The SEAM project was a move in the right direction for providing access to complex models for industry benchmarks and educational purposes. This SEG endeavor has proved a success as revealed by a series of subsequently published papers (e.g., Stefani et al., 2010; Fehler and Keliher, 2011; Capello, 2017). However, the phase 1 model from SEAM, for instance, is limited to deep-water allochthonous salt geology for the Gulf of Mexico, which may not be appropriate for understanding different geologic scenarios.

Manuscript received by the Editor 15 June 2018; revised manuscript received 30 March 2019; published ahead of production 29 May 2019; published online 12 August 2019.

¹PETROBRAS-EXP/GEOF/MNS, Av. República do Chile 330, Torre Leste, 11° andar, Rio de Janeiro, RJ 20031-170, Brazil. E-mail: jorlivan@petrobras.com.br.

²PETROBRAS-EXP/GEOF/MNS, Av. República do Chile 330, Torre Leste, 11° andar, Rio de Janeiro, RJ 20031-170 Brazil and DGAP/FGEL/UERJ, Rua São Francisco Xavier 524, 2029a, Rio de Janeiro, RJ 20550-013, Brazil. E-mail: ptarsomenezes@gmail.com.

© 2019 Society of Exploration Geophysicists. All rights reserved.

Another open-source model is Marlim R3D (MR3D), which is a project aiming to provide a realistic geoelectric model for the deep-water turbidites reservoir system of the Brazilian continental margin. These are considered analogs to several other systems around the world, such as those at the African continental margin. In phase 1, [Carvalho and Menezes \(2017\)](#) discuss the workflow on how they have built the model and made it freely available for research or commercial use. Presently, in phase 2, we perform a suite of CSEM finite-difference 3D simulations on the MR3D resistivity model. We aim to produce a full-azimuth 3D CSEM data set that not only sim-

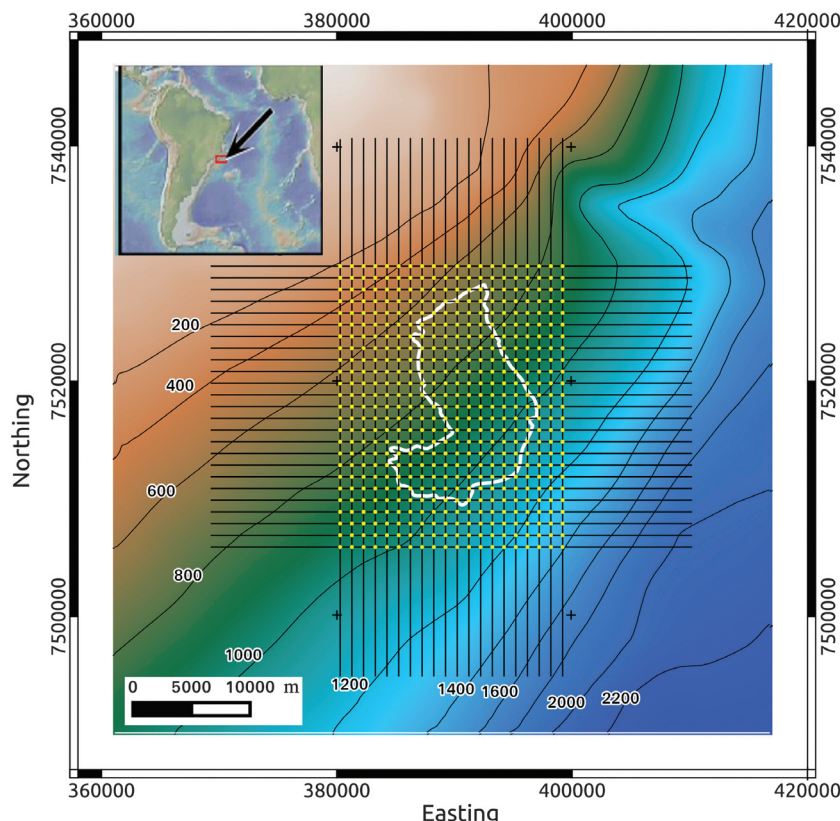


Figure 1. The CSEM acquisition geometry superimposed on the bathymetric map of the MR3D area. The Marlim reservoir outline is shown in the white line. The yellow dots are the receiver locations distributed in a 1000 m spacing regular grid. The black lines are the source towlines evenly spaced at 1000 m. Source locations are spaced every 100 m along each towline.

Table 1. The MR3D resistivity ranges ([Carvalho and Menezes, 2017](#)).

MR3D resistivities

Lithology	Rh ($\Omega \cdot \text{m}$)	Rv ($\Omega \cdot \text{m}$)
Oligo-Miocene shales	1.0	2
Marlim turbidites	70	140
Postsalt carbonates	6.5	13
Salt	1000	1000
Presalt carbonates	15	30

ulates current acquisitions patterns but also, in most circumstances, exceeds them.

The MR3D CSEM synthetic data set herein introduced can be used to support and eventually enhance 3D forward and inversion modeling studies and also subsurface imaging and characterization techniques using electromagnetic data alone or coupled with other types of geophysical data. The produced CSEM data for a wide frequency range (0.125–1.25 Hz) can also be used to assess a priori the effectiveness of a given CSEM interpretation workflow.

The CSEM data are simulated from the MR3D model using a full-azimuth geometry (see Figure 1) with north-south and east-west towlines and a large number of deployed receivers (500 Rx). Comparing this geometry with conventional CSEM acquisitions enables the evaluation of alternative geometries and, thus, helps suggest parameters for optimal survey designs.

MR3D RESISTIVITY MODEL

In the Brazilian continental margin, sand-rich turbidites compose the most important postsalt reservoir rocks at several oilfields and, consequently, possible targets for CSEM surveys ([Bueno et al., 2014](#)). These turbidites were deposited in deepwater settings associated with slope and continental rise deposits ([Freire, 1989](#)).

MR3D is a realistic anisotropic geoelectric model that aims to be a benchmark for CSEM studies of the turbiditic reservoirs offshore Brazil ([Carvalho and Menezes, 2017](#)). The model, based on the previous seismic interpretation ([Nascimento et al., 2014](#)), includes fine-scale stratigraphy and fluid-filled reservoirs. Marlim has a variable thickness of up to 80 m, with a mean of 50 m. The volume of interest of the model measures 27 km north-south by 24 km east-west by 6 km depth ([Carvalho and Menezes, 2017](#)).

The vertical transverse anisotropy (VTI) model can adequately represent the low-angle dipping Mio-Oligocene sediments. To more complex tilted anisotropic geologies, a tilted transverse isotropic model would be more adequate ([Davydycheva and Frenkel, 2013](#)). An anisotropic ratio (Rv/Rh) of two was assigned to the whole sedimentary section, except for the autochthonous salt layer,

which is outlined by a 1000 $\Omega \cdot \text{m}$ isotropic and homogeneous layer (Table 1). The anisotropy ratio is routinely found in several triaxial induction logs in the Brazilian offshore basins ([Menezes, 2013](#)).

The simplified VTI model was originated from P-wave seismic velocities V_p interpolated along the main stratigraphic horizons in the studied area via the horizon cube methodology ([de Groot et al., 2010](#)). Details about the petrophysical modeling in the development of the MR3D resistivity model are given by [Carvalho and Menezes \(2017\)](#).

Figure 2 shows the vertical resistivity extracted along a horizon slice at the top of the reservoir. The Marlim reservoir facies (clean sandstones) appears as a high-resistivity body embedded in a low-resistivity background (marls and shales). Rather than a single resistivity body, MR3D presents a complex resistivity pattern that

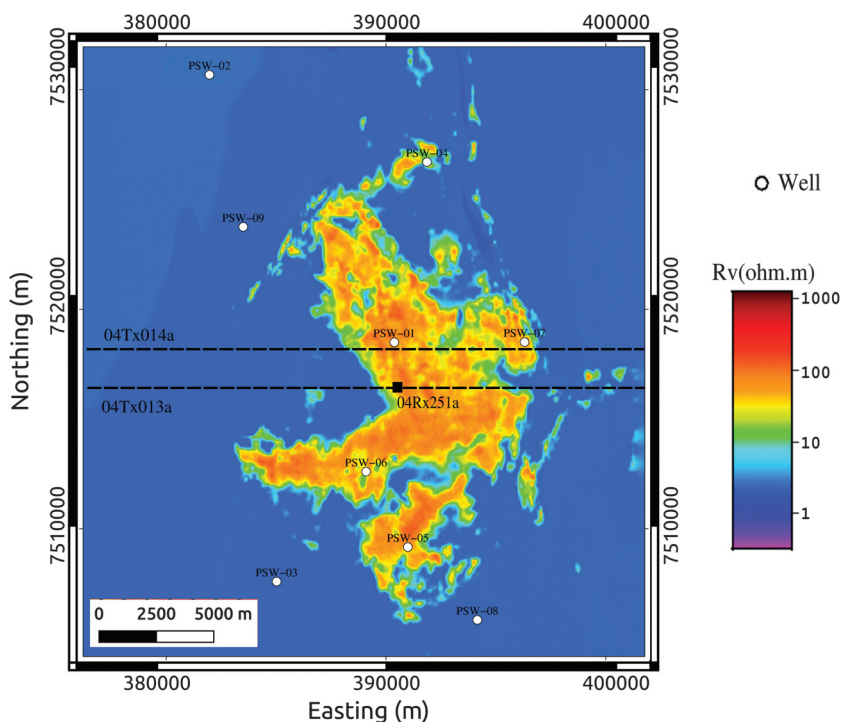


Figure 2. Map of the MR3D vertical resistivity (R_v) distribution along the Oligocene horizon (top of reservoir). PSW-01 to PSW-09 are the available wells provided by Carvalho and Menezes (2017). The Marlim turbidites (clean sandstones) are clearly highlighted as high-resistivity bodies. The dashed lines 04Tx013 and 04Tx014 are east–west towlines.

represents a genuine challenge for CSEM imaging. In addition to the main reservoir, there are other smaller turbidites bodies at various stratigraphic levels in the Oligo-Miocene range. Figure 3 shows a vertical cross section of the R_v model along the east–west towline Tx13. The Marlim reservoirs (M in Figure 3) are described as thin high-resistive bodies at 2900 m in depth.

3D MESH

We conducted the 3D forward modeling using a parallelized commercial fast finite-difference time-domain (FDTD) CSEM modeling algorithm (Maaø, 2007). The same code was adopted in the SEAM project (Stefani et al., 2010). We used an anisotropic

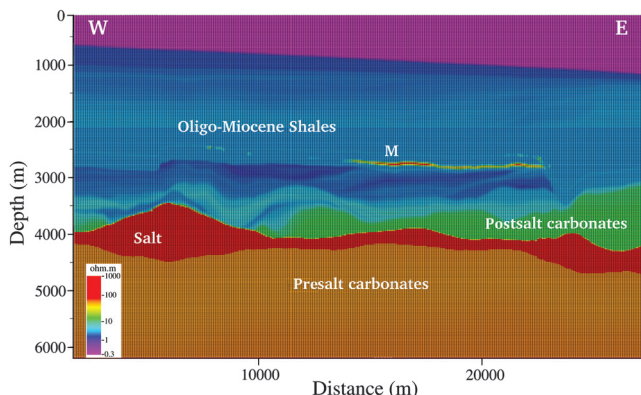


Figure 3. Cross section of the MR3D vertical resistivity along the east–west towline 04Tx013. Marlim oil-prone turbidites (M) appear as thin resistive bodies.

model containing the horizontal (R_h) and vertical (R_v) resistivities including the seafloor bathymetry with a $0.32 \Omega \cdot m$ isotropic water layer. The model comprises a volume of $56 \times 51 \times 6$ km, and it is finely discretized at regular intervals of $100 \times 100 \times 20$ m. Such refinement is necessary to properly represent the thin and discontinuous turbidites reservoirs (Figure 3). The air layer was included in our simulations via a non-local boundary condition at the water-air interface (Wang and Hohmann, 1993; Mittet, 2010).

The mesh discretization led to an FDTD mesh with almost 90 million cells (Table 2). The modeling exercises were executed using 62 core processors of our local Intel Xeon E5-2690 v2 @ 3.00 GHz cluster (3968 GB memory per node) with a runtime of approximately 9 h for each experiment.

CSEM ACQUISITION GEOMETRY

Full-azimuth CSEM data were simulated for a total of 500 receivers located on the irregular seafloor of the MR3D model. For each receiver, sources were located along 45 towlines having a spacing of 1000 m. Towlines were positioned along 25 east–west lines and 20 north–south lines for each receiver. Figure 1 shows the

Table 2. Finite-difference mesh used in the MR3D forward-modeling exercise.

MR3D mesh	
Cell size — X	100 m
Cell size — Y	100 m
Cell size — Z	20 m
Number of cells — X	563
Number of cells — Y	511
Number of cells — Z	310
Total number of cells	89,882,950

Table 3. Source acquisition parameters of the MR3D experiment.

Source parameters	
Pitch	0°
Feathering	0°
Dipole length	278 m
Current	1250 A
Offset step	100 m
Offset range	500–11,000 m
Altitude above sea level	50 m

receiver positions and towlines superimposed on the bathymetry of the MR3D model.

Each east–west towline has a length of 42 km, and each north–south towline has a length of 47 km. Both directions are extending 11 km away from the first and last receivers at each towline (our

volume of interest). Source positions were spaced at 100 m along each towline for a total of 201 source positions along each towline. The source is a 278 m long horizontal electrical dipole, oriented parallel to the towline. The source parameters of the MR3D experiment are summarized in Table 3.

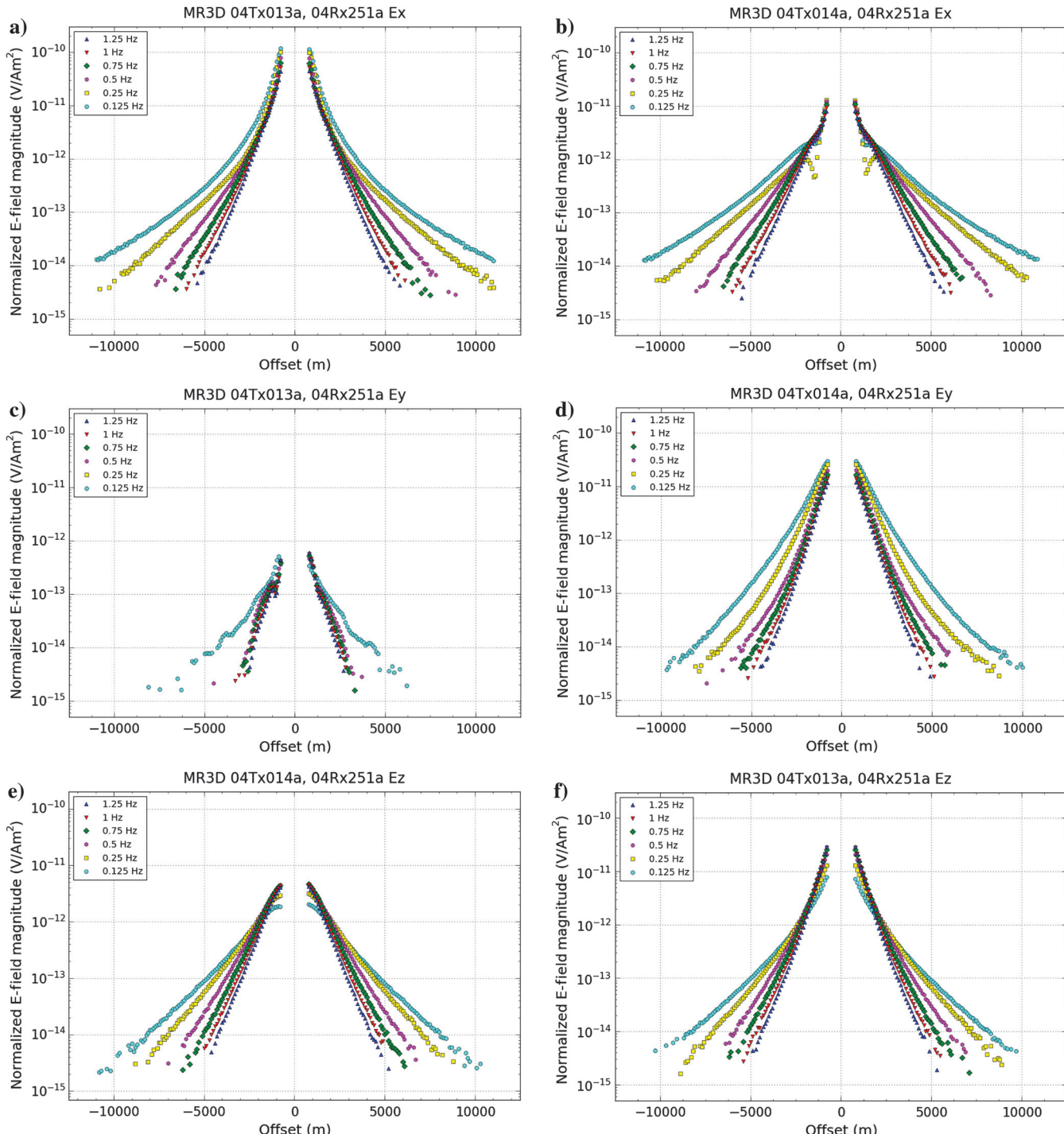


Figure 4. Typical data for the MR3D survey showing the overall good quality of the inline and broadside electric fields. Inline E_x , E_y , and E_z fields at site 04Rx251a (towline 04Tx013a) are shown in (a, c, and e), respectively. Broadside E_x , E_y , and E_z fields at site 04Rx251a (towline 04Tx014a) are shown in (b, d, and f), respectively.

CSEM DATA

We simulated all six electromagnetic field components E_x , E_y , E_z , H_x , H_y , and H_z for six source frequencies of 0.125, 0.25, 0.5, 0.75, 1, and 1.25 Hz. These frequencies are within the frequency range of the largest multiclient CSEM campaign over the Brazilian offshore margin. In total, the CSEM data set covered more than 5000 km² over several basins, including the Campos Basin (Lorenz et al., 2013).

The electromagnetic fields of the noise-free data were calculated with 0.1 s time steps, at a maximum number of 200,000 time steps,

and convergence accuracy of 10^{-4} . We normalized the electric fields by the dipole moment. Then, we added multiplicative noise with a 1% standard deviation following the approach of Mittet and Morten (2012), and we set a 10^{-15} V/Am² and 10^{-12} 1/m² ambient noise level for the normalized electric and magnetic fields, respectively. The output data set was generated in the current industry network common data form-based data format (Zach and Frenkel, 2012). The modeling resulted in high-quality inline and broadside data to a source-receiver offset of 11 km, but maximum ranges of 5–6 km were typical for higher frequencies (Figure 4).

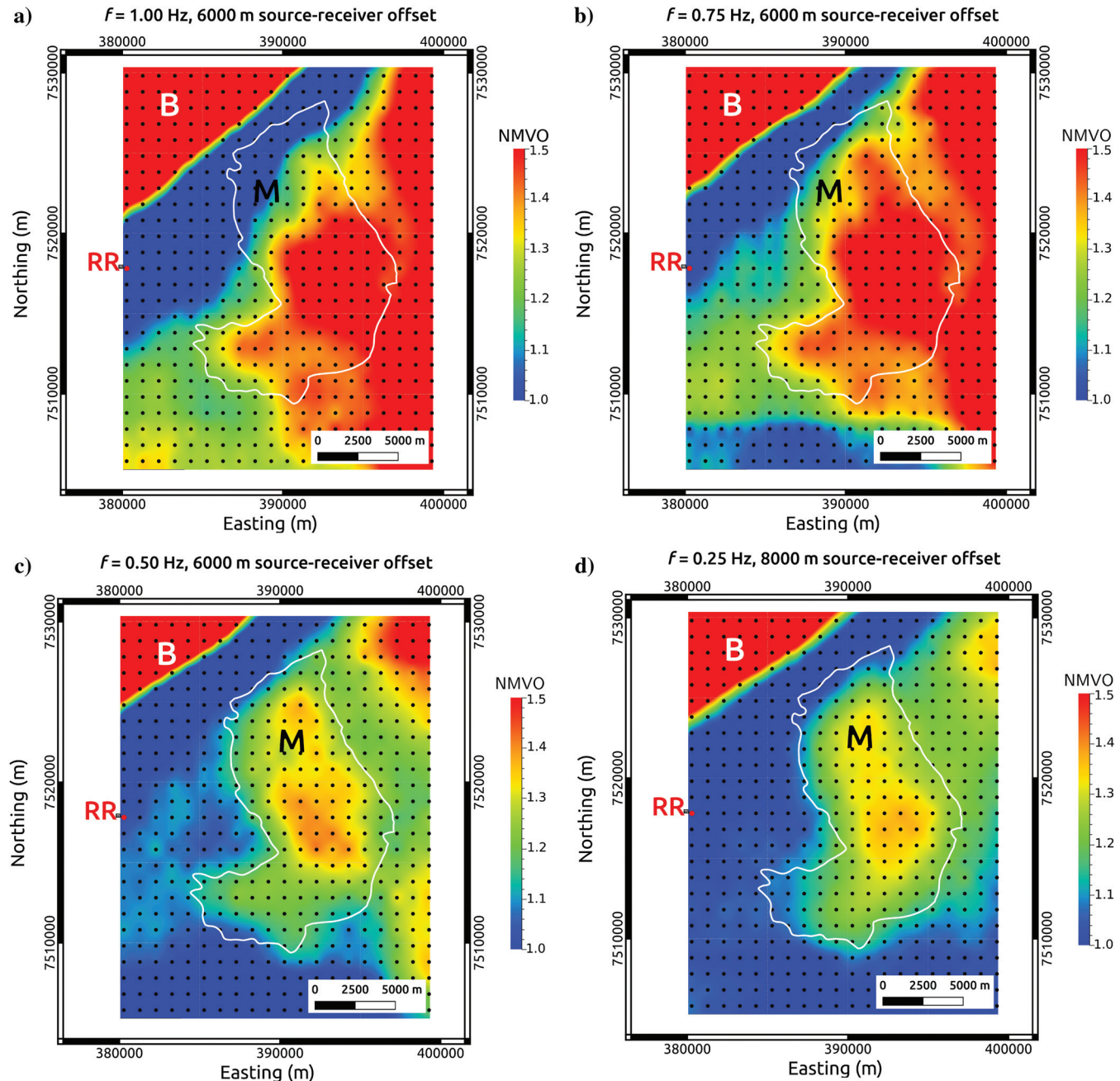


Figure 5. Inline electric field normalized magnitude versus offset (NMVO) maps at different frequencies and offsets: (a) 1.00 Hz and 6000 m offset, (b) 0.75 Hz and 6000 m offset, (c) 0.50 Hz and 6000 m offset, and (d) 0.25 Hz and 8000 m offset. The Marlim reservoir exhibits anomalous values up to 50% above the background at 6000–8000 m offsets. The black circles indicate the positions of the receivers at the seabed. RR (the red circle) is the reference receiver 04Rx241a that images the background resistivity.

A standard preliminary step in CSEM interpretation is the use of data normalization to generate pseudosections along a chosen line or anomaly maps at fixed constant offsets. These provide, respectively, to the interpreters a first hint about the existence or not of a given resistor in depth or area. There are several ways to perform CSEM qualitative interpretation, and we have chosen the reference receiver normalization technique (Buonora et al., 2014). Our reference receiver of choice was 04Tx241a (RR in Figure 5) because it is located in a portion of the model that contains only the background resistivity (i.e., the regional geology surrounding the reservoir). In this procedure, data from each receiver at a given frequency are divided by the reference receiver data and plotted in pseudosections and/or maps at a fixed offset.

In Figure 5, we present the inline electric field normalized magnitude maps at four frequencies and offsets: 1.00 Hz with 6000 m offset (Figure 5a), 0.75 Hz with 6000 m offset (Figure 5b), 0.50 Hz with 6000 m offset (Figure 5c), and 0.25 Hz with 8000 m offset (Figure 5d). The Marlim reservoir boundary is displayed to help guide the interpretation. In all frequencies, the strongest anomaly appears in the northwestern portion of the area (B in Figure 5). We associate this anomaly with the bathymetric effect. The appearance of spurious anomalies is one of the drawbacks of the reference receiver normalization technique (Buonora et al., 2014). In that portion of the studied area, there is a seafloor rise and anomaly B follows the bathymetric contours as shown in Figure 1.

Marlim is represented by a resistive anomaly that matches well the reservoir's boundaries in the frequency range of 1.00–0.25 Hz. This is particularly true in its western, northern, and southern sides (Figure 5a–5d). In the eastern portion of the area, the boundary definition is poorly outlined due to the existence of resistive anomalies correlated with other smaller turbidite reservoirs in the eastward portion of the studied model (Carvalho and Menezes, 2017). These anomalies are stronger in the high-frequency range (1.00–0.75 Hz) than in the low frequencies (0.50–0.25 Hz) as shown in Figure 5. This is an indication that these small turbidite bodies are relatively shallower than the Marlim reservoir.

CONCLUSION

MR3D is a realistic geoelectric model for CSEM simulations that aims to be a benchmark model for studies of the postsalt turbiditic reservoirs at the Brazilian offshore margin.

We developed a detailed 3D CSEM finite-difference time-domain forward study to generate an official CSEM data set for the MR3D model. To that end, we simulated a full-azimuth survey with 45 tow-lines striking in the north–south and east–west directions over a total of 500 receivers evenly spaced at 1 km intervals along the rugged seafloor of the MR3D model. To properly represent the thin, discontinuous, and complex geometries of the studied reservoirs, we have built a finely X , Y , and Z discretized mesh of $100 \times 100 \times 20$ m, respectively. As a result, we obtained a substantially sized mesh, with a total of approximately 90 million cells.

We modeled all six electromagnetic field components for six source frequencies in the range of 0.125–1.25 Hz. A multiplicative noise with a 1% standard deviation was added to the data. The full CSEM data set, with inline and broadside data, for the six electromagnetic fields and six frequencies, is freely available to the general public on the Zenodo platform.

Following the successful guideline provided by the SEAM project, we are extending the MR3D project to include seismic,

gravity, and magnetotelluric simulations. In the future, all of these data will also be publicly available. Hence, our CSEM data set may, shortly, be evaluated individually or within multiphysics interpretation schemes.

ACKNOWLEDGMENT

We want to acknowledge GEOPHYSICS' assistant editor E. Gasperikova, associate editor C. Farquharson, and three anonymous reviewers for the valuable suggestions that helped to improve our paper. We thank Petrobras for its support and permission to publish this paper. We acknowledge M. Mallman and M. Ribas for their assistance to adjust our figures. P. T. L. Menezes appreciates the support provided by a research grant from CNPq.

DATA AND MATERIALS AVAILABILITY

The synthetic CSEM data are freely available for research or commercial use under the Creative Common License at the Zenodo platform (<https://zenodo.org/>). A noise-free data set is provided at <https://doi.org/10.5281/zenodo.1807135>, and a 1% added noise data set is available at <https://doi.org/10.5281/zenodo.1256787>.

REFERENCES

- Bhuyian, A., B. Thrane, M. Landrø, and S. Johansen, 2010, Controlled source electromagnetic three-dimensional grid-modelling based on a complex resistivity structure of the seafloor: Effects of acquisition parameters and geometry of multi-layered resistors: *Geophysical Prospecting*, **58**, 505–533, doi: [10.1111/j.1365-2478.2009.00844.x](https://doi.org/10.1111/j.1365-2478.2009.00844.x).
- Buonora, M. P. P., J. L. Correa, L. S. Martins, P. T. L. Menezes, E. J. C. Pinho, J. L. Silva Crepaldi, M. P. P. Ribas, S. M. Ferreira, and R. C. Freitas, 2014, mCSEM data interpretation for hydrocarbon exploration: A fast interpretation workflow for drilling decision: *Interpretation*, **2**, no. 3, SH1–SH11, doi: [10.1190/INT-2013-0154.1](https://doi.org/10.1190/INT-2013-0154.1).
- Capello, M. A., 2017, Introduction to this special section: Celebrating 10 years of SEAM success: *The Leading Edge*, **36**, 723–723, doi: [10.1190/tle36090723.1](https://doi.org/10.1190/tle36090723.1).
- Carvalho, B. R., and P. T. L. Menezes, 2017, Marlim R3D: A realistic model for CSEM simulations — Phase I: Model building: *Brazilian Journal of Geology*, **47**, 633–644, doi: [10.1590/2317-4889201720170088](https://doi.org/10.1590/2317-4889201720170088).
- Colombo, D., D. Rovetta, and E. Turkoglu, 2018, CSEM-regularized seismic velocity inversion: A multiscale, hierarchical workflow for subsalt imaging: *Geophysics*, **83**, no. 5, B241–B252, doi: [10.1190/geo2017-0454.1](https://doi.org/10.1190/geo2017-0454.1).
- Constable, S., and L. J. Srnka, 2007, An introduction to marine controlled-source electromagnetic methods for hydrocarbon exploration: *Geophysics*, **72**, no. 2, WA3–WA12, doi: [10.1190/1.2432483](https://doi.org/10.1190/1.2432483).
- Davydycheva, S., and M. A. Frenkel, 2013, The impact of 3D tilted resistivity anisotropy on marine CSEM measurements: *The Leading Edge*, **32**, 1374–1381, doi: [10.1190/tle32111374.1](https://doi.org/10.1190/tle32111374.1).
- de Groot, P., A. Huck, G. de Bruin, N. Hemstra, and J. Bedford, 2010, The horizon cube: A step change in seismic interpretation!: *The Leading Edge*, **29**, 1048–1055, doi: [10.1190/1.3485765](https://doi.org/10.1190/1.3485765).
- Dunham, M. W., S. Ansari, and C. G. Farquharson, 2018, Application of 3D marine controlled-source electromagnetic finite-element forward modeling to hydrocarbon exploration in the Flemish Pass Basin offshore Newfoundland, Canada: *Geophysics*, **83**, no. 2, WB33–WB49, doi: [10.1190/geo2017-0451.1](https://doi.org/10.1190/geo2017-0451.1).
- Fanavoll, S., P. T. Gabrielsen, and S. Ellingsrud, 2014, CSEM as a tool for better exploration decisions: Case studies from the Barents Sea, Norwegian Continental Shelf: *Interpretation*, **2**, no. 3, SH55–SH66, doi: [10.1190/INT-2013-0171.1](https://doi.org/10.1190/INT-2013-0171.1).
- Fehler, M., 2009, SEAM Phase I progress report: Classic data sets: *The Leading Edge*, **28**, 1178–1181, doi: [10.1190/tle28101178.1](https://doi.org/10.1190/tle28101178.1).
- Fehler, M., and P. J. Keliher, 2011, SEAM Phase I: Challenges of subsalt imaging in tertiary basins, with emphasis on deepwater Gulf of Mexico: SEG.
- Freire, W., 1989, Campos basin deepwater giant fields: Presented at the Offshore Technology Conference.
- Lorenz, L., H. T. Pedersen, and M. P. Buonora, 2013, First results from a Brazilian mC-SEM calibration campaign: 13th International Congress of the Brazilian Geophysical Society and EXPOGEF, 131–136.

- Løseth, L. O., T. Wiik, P. A. Olsen, and J. O. Hansen, 2014, Detecting Skrugard by CSEM — Prewell prediction and postwell evaluation: Interpretation, **2**, no. 3, SH67–SH77, doi: [10.1190/INT-2013-0152.1](https://doi.org/10.1190/INT-2013-0152.1).
- Maaø, F. A., 2007, Fast finite-difference time-domain modeling for marine-subsurface electromagnetic problems: Geophysics, **72**, no. 2, A19–A23, doi: [10.1190/1.2434781](https://doi.org/10.1190/1.2434781).
- Menezes, P. T. L., 2013, Fundamentos do metodo magnetotelhrico na exploracao de petroleo: Sociedade Brasileira de Geofisica.
- Miotti, F., A. Zerilli, P. T. L. Menezes, J. L. S. Crepaldi, and A. R. Viana, 2018, A new petrophysical joint inversion workflow: Advancing on reservoirs characterization challenges: Interpretation, **6**, no. 3, SG33–SG39, doi: [10.1190/INT-2017-0225.1](https://doi.org/10.1190/INT-2017-0225.1).
- Mittet, R., 2010, High-order finite-difference simulations of marine CSEM surveys using a correspondence principle for wave and diffusion fields: Geophysics, **75**, no. 1, F33–F50, doi: [10.1190/1.3278525](https://doi.org/10.1190/1.3278525).
- Mittet, R., and J. P. Morten, 2012, Detection and imaging sensitivity of the marine CSEM method: Geophysics, **77**, no. 6, E411–E425, doi: [10.1190/geo2012-0016.1](https://doi.org/10.1190/geo2012-0016.1).
- Nascimento, T. M., P. T. L. Menezes, and I. L. Braga, 2014, High-resolution acoustic impedance inversion to characterize turbidites at Marlim Field, Campos Basin, Brazil: Interpretation, **2**, no. 3, T143–T153, doi: [10.1190/INT-2013-0137.1](https://doi.org/10.1190/INT-2013-0137.1).
- Orange, A., K. Key, and S. Constable, 2009, The feasibility of reservoir monitoring using time-lapse marine CSEM: Geophysics, **74**, no. 2, F21–F29, doi: [10.1190/1.3059600](https://doi.org/10.1190/1.3059600).
- Puzeyrev, V., J. Koldan, J. de la Puente, G. Houzeaux, M. Vazquez, and J. M. Cela, 2013, A parallel finite-element method for three-dimensional controlled-source electromagnetic forward modeling: Geophysical Journal International, **193**, 678–693, doi: [10.1093/gji/ggt027](https://doi.org/10.1093/gji/ggt027).
- Ray, A., D. L. Alumbaugh, G. M. Hoversten, and K. Key, 2013, Robust and accelerated Bayesian inversion of marine controlled-source electromagnetic data using parallel tempering: Geophysics, **78**, no. 6, E271–E280, doi: [10.1190/geo2013-0128.1](https://doi.org/10.1190/geo2013-0128.1).
- Stefani, J., M. Frenkel, N. Bundalo, R. Day, and M. Fehler, 2010, SEAM update: Models for EM and gravity simulations: The Leading Edge, **29**, 132–135, doi: [10.1190/tle29020132.1](https://doi.org/10.1190/tle29020132.1).
- Tseng, H.-W., J. Stalnaker, L. M. MacGregor, and R. V. Ackermann, 2015, Multidimensional analyses of the SEAM controlled source electromagnetic data — The story of a blind test of interpretation workflows: Geophysical Prospecting, **63**, 1383–1402, doi: [10.1111/1365-2478.12327](https://doi.org/10.1111/1365-2478.12327).
- Wang, T., and G. W. Hohmann, 1993, A finite-difference, time-domain solution for three dimensional electromagnetic modeling: Geophysics, **58**, 797–809, doi: [10.1190/1.1443465](https://doi.org/10.1190/1.1443465).
- Yoon, D., M. S. Zhdanov, J. Mattsson, H. Cai, and A. Gribenko, 2016, A hybrid finite-difference and integral-equation method for modeling and inversion of marine controlled-source electromagnetic data: Geophysics, **81**, no. 5, E323–E336, doi: [10.1190/geo2015-0513.1](https://doi.org/10.1190/geo2015-0513.1).
- Zach, J. J., and M. A. Frenkel, 2012, 3D inversion-based interpretation of marine CSEM data: SPE Reservoir Evaluation and Engineering, **15**, 321–334, doi: [10.2118/158810-PA](https://doi.org/10.2118/158810-PA).